

Ekrem Gulsevincler¹, Mustafa Resit Usal², Demet Yilmaz³

¹ Kastamonu University, Electric and Energy Department, Abana Sabahat Mesut Yilmaz Vocational School, 37970 Kastamonu, Turkey

² Suleyman Demirel University, Department of Mechanical Engineering, Faculty of Engineering, 32260 Isparta, Turkey

³ Suleyman Demirel University, Department of Textile Engineering, Faculty of Engineering, 32260 Isparta, Turkey

Modular Jet-Ring Yarn Spinning System

Modularni sistem za izdelavo curkovne prstanske preje

Original scientific article/Izvirni znanstveni članek

Received/Prispelo 2-2020 • Accepted/Sprejeto 4-2020

Abstract

In this study, a modular nozzle design was developed in which the twist chamber diameter, injector diameter, injector angle and the number of injectors of the nozzle can be optionally changed without the need of conventional manufacturing methods. The developed modular nozzle was compared with conventional nozzles taking into account both experimental and numerical analysis results. Experimental performance tests were conducted on the yarn quality achieved using air twist, which is the subject of the application of the nozzle. In the experimental study, conventional nozzles with the same structural configurations were produced to determine modular nozzle performance. In all jet-ring yarn productions, the air pressure was set at two different values: 75 kPa and 125 kPa (gauge). Yarn hairiness, irregularity and imperfection tests were carried out using an Uster Tester 3. Tensile properties (percentage of elongation and tenacity measured as cN/tex) tests were carried out using an Uster Tensorapid. In the numerical analysis, an Ansys CFX 18.0 computational fluid dynamics program was used for both conventional nozzle and modular nozzle configurations. All parametric study configurations were set separately using an SST turbulence model. Comparing the flow parameters of yarn hairiness (CFD analysis), it was found that increasing vorticity or helicity real eigen values reduced yarn hairiness.

Keywords SST, swirling flow, swirl number, jet-ring, nozzle-ring, air nozzle

Izvleček

V študiji je bila razvita modularno zasnovana šoba za curkovno predenje prstanske preje, v kateri se lahko poljubno spreminjajo premer vijne komore, premer in kot injektorja. Število injektorjev v šobi se lahko spreminja brez potrebe po običajnih proizvodnih metodah. Razvita modularna šoba je primerjana z običajnimi šobami z upoštevanjem rezultatov eksperimentalne in numerične analize. Izvedeni so bili eksperimentalni preizkusi kakovosti preje, vitič z uporabo modularno zasnovane šobe. Za določitev uporabnosti modularne šobe so bile izdelane običajne šobe z enakimi strukturnimi konfiguracijami. V vseh primerih izdelave curkovne prstanske preje sta bili uporabljene dve vrednosti zračnega tlaka, in sicer 75 kPa ter 125 kPa. Na Uster Testerju 3 so bile izvedene meritve kosmatosti in neenakomernosti preje ter količine napak v preji. Natezne lastnosti (pretržna napetost in pretržni raztezek) so bile določene na aparatu Uster Tensorapid. Za numerično analizo običajne konfiguracije šobe in modularne šobe je bil uporabljen računalniški program za računalniško dinamiko tekočin, Ansys CFX 18.0. Vse študije konfiguracionih parametrov so bile izvedene ločeno z uporabo SST turbulentnega modela. Z analizo CFD, ki omogoča računalniško primerjavo parametrov dinamike tekočin, je bilo ugotovljeno, da povečanje vrtinčenja ali vijačenja realno zmanjša vrednosti kosmatost preje.

Ključne besede: SST, vrtinčasti tok, vrtinčna številka, curek-prstan, obroč šobe, zračna šoba

Corresponding author/Korespondenčna avtorica:

Dr. Ekrem Gulsevincler

E-mail: egulsevincler@kastamonu.edu.tr

ORCID: 0000-0002-4787-6275

Tekstilec, 2020, 63(2), 80-93

DOI: 10.14502/Tekstilec2020.63.80-93

1 Introduction

Swirling flows are found in many areas of our lives and engineering. ‘Swirling flow’ [1] is defined as the rotating helical flow and can be seen in natural events, e.g. tornadoes, hurricanes, water vents, etc. Another example of swirling flows are the air-jet nozzles used in the textile industry on spinning machines. Swirling air flow is produced in an air nozzle depending on nozzle geometry and compressed air [2, 3]. The helical rotating flow in turbulent jets results in an increase in jet growth, drift speed and the decay rate of the jet. These effects also increase when helical rotation density increases. Swirling flows depend on different parameters, most of which were formulated and found as a result of studies. The most important parameter is the swirling number (S_n). The integral definition of the swirling number is expressed as the ratio of the axial flux of the angular momentum to the axial momentum flux and radius multiplication [1].

$$S_n = \frac{\text{Angular Momentum}}{R \cdot \text{Axial Momentum}} = \frac{G_{Ang}}{RG_{Ax}} = \frac{\int_0^{2\pi} \int_0^R u_z u_\phi r^2 dr d\phi}{R \int_0^{2\pi} \int_0^R u_z^2 r dr d\phi} \quad (1)$$

where R represents the twisting chamber radius, u_z represents the axial velocity component, u_ϕ represents the tangential velocity component, and r and ϕ represent the radial and angular coordinates taken according to the main hole (twisting chamber) centre. Since these values cannot be known in advance, a geometric swirling number (S_g) can also be defined based on the ratio of mass flows in the twisting chamber and in the entrance cross-sectional areas. These values can also be defined in a geometric swirling number (S_g) based on the ratio of mass flows in the twisting chamber and in the air inlet entrance (injectors) cross-sectional areas, as it is not known before the CFD (computational fluid dynamics) analysis or experimental studies are performed [1].

$$S_g = \left(\frac{m_t}{m_T} \right)^2 \left(\frac{D_{tc}}{d} \right)^2 \frac{\sin\theta}{N} \quad (2)$$

where m_t and m_T represent mass flows in the injectors (total) and in the test section (twisting chamber). According to equation 2, the geometric swirling number (i.e. the swirl density) depends on the diameter of the twist chamber D_{tc} , injector diameter d , injector angle θ and the number of injectors N [1].

1.1 CFD turbulence model used

The calculation of the turbulent helical rotating flow by computational fluid dynamics is the determining factor for the appropriate turbulence model. The swirling number is a decisive factor for the turbulence model of the turbulent helical rotating flow in the analysis of computational fluid dynamics. Literature suggests that if the swirling number is less than 0.5, there is a weak or medium swirling flow that is sufficient for the flow analysis, and the k- ϵ turbulence model can be used (with realisable k- ϵ , RNG k- ϵ selections). Guo [1] reported that the Reynolds Stress Model (RSM) is generally more reliable than two-equation models, but the RSM model needs a large memory and high processor time, and convergence is more difficult. As an alternative, the realisable k- ϵ turbulence model closes the turbulent Navier-Stokes equations. The realisable k- ϵ model is a revised k- ϵ turbulence model. Compared to the standard k- ϵ turbulence model, the realisable k- ϵ model exhibits superior performance for flows involving boundary layers, flow separations and rotation under strong reverse pressure gradients. In another turbulent swirling flow study, turbulence models were compared using a steady flow analysis, and an SST (Shear Stress Transport) turbulence model was found to be closest to the experimental study.

The SST includes a collation function to add a cross-diffusion term in the ω equation in the turbulence model and to ensure that model equations behave appropriately in the near-wall and far area regions [4]. The SST turbulence model basically has the same definition as the k- ω model [4–6]:

$$\frac{\partial}{\partial t}(\rho k) + \frac{\partial}{\partial x_i}(\rho k u_i) = \frac{\partial}{\partial x_j} \left(\Gamma_k \frac{\partial k}{\partial x_j} \right) + G_k - Y_k + S_k \quad (3)$$

and

$$\begin{aligned} \frac{\partial}{\partial t}(\rho \omega) + \frac{\partial}{\partial x_i}(\rho \omega u_i) &= \\ &= \frac{\partial}{\partial x_j} \left(\Gamma_\omega \frac{\partial \omega}{\partial x_j} \right) + G_\omega - Y_\omega + D_\omega + S_\omega \end{aligned} \quad (4)$$

where G_k represents the production of turbulence kinetic energy due to average velocity gradients. G_ω represents the production of ω . Γ_k and Γ_ω represent the effective diffusivity of k and ω . Y_k and Y_ω represent the dissipation of k and ω owing to turbulence. D_ω is the cross-diffusion term formulated in equation 21. S_k and S_ω are user-defined resource terms [4–11].

1.2 Jet-ring (nozzle-ring) spinning system

This system is based on the placement of air nozzles used in the air-jet spinning system between the output system of the conventional ring spinning system and the yarn guide system, called jet-ring or nozzle-ring (Figure 1). Air is fed into the air nozzle used in the jet-ring system at a certain pressure value. Compressed air leads to a rotating air vortex in the nozzle. The air vortex ensures that the fibre ends that protrude outward from the yarn body are wound up in the yarn body, thereby reducing yarn hairiness [12]. In addition to low yarn hairiness, fabrics made from the aforementioned yarns are smoother and more resistant to pilling than the fabrics made from conventional ring spun yarns [3]. Air nozzles thus provide improved yarn properties and long-term advantages due to the improvements in fabric performance.

The first experiments with the jet-ring or nozzle-ring spinning system were carried out towards the end of the 1990s by Wang et al. [3]. Recently, many researchers have been working on yarn properties, in particular on the improvement of yarn hairiness over the use of air nozzles in a conventional ring spinning system [2, 3, 11–16].



Figure 1: Application of an air nozzle on a jet-ring spinning system

2 Materials and methods

2.1 Conventional jet-ring air nozzle

Conventional jet-ring (nozzle-ring) systems have a similar construction to compact-jet systems [2, 12], while siro-jet [13, 14] spinning systems are composed of three basic components as follows: compressed air, nozzle and yarn. Compressed air with a certain value from the air compressor is transported to the level and passed through the thread. The nozzle assembly (Figure 2c) has a very simple structure and consists of a nozzle housing (Figure 2a) and nozzle body (Figure 2b). The nozzle body part has a circular cross-section consisting of the main hole (twisting chamber) (1), injectors (2), connecting screw for the nozzle housing (3) and the nozzle outlet (4) (Figure 2b). The main hole extends from the nozzle entrance to the nozzle outlet. The injectors are positioned to be tangential to the twisting chamber. The nozzle housing conveys the compressed air from the air compressor to the twisting chamber section of the device via the injectors.

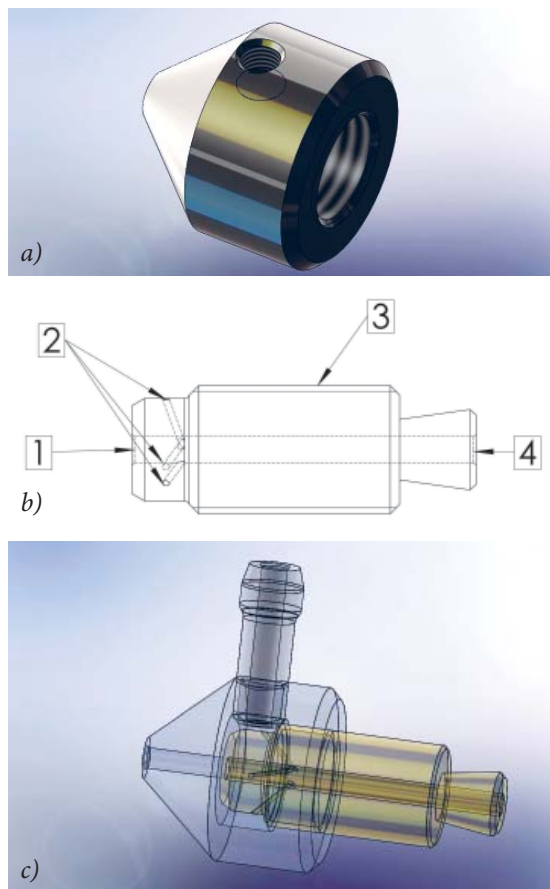


Figure 2: Nozzle (a) housing, (b) body and (c) assembly

Flow volume is illustrated in Figure 3. As shown in Figure 3, the design parameters of the air nozzles are composed of twist chamber diameter (D_{tc}), injector diameter (D_i) and injector angle (θ). The conventional jet-ring nozzle length is 27 mm, injector diameter is $\phi = 0.5$ mm, injector quantity is 3 and twisting chamber diameter is $\phi = 3$ mm. Those measurements were maintained for all samples.

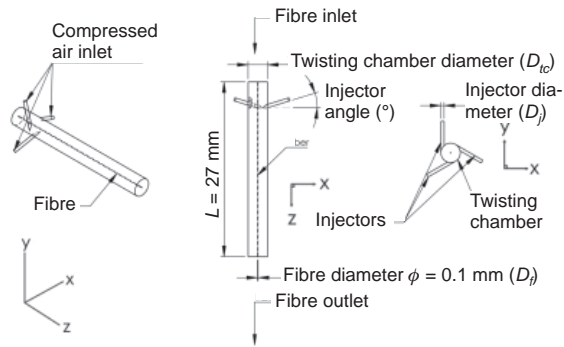


Figure 3: 3D model drawing of a conventional nozzle flow volume with 3 injectors

2.2 Modular jet-ring air nozzle

In the event of any structural parameter change in the conventional jet-ring air nozzle, a nozzle specific to that parameter must be produced and the existing nozzle removed and reassembled. This leads to costs for new nozzle parts, additional labour and labour costs. In the light of these shortcomings, a design was developed in this study, in which the twist chamber diameter, injector diameter, injector angle and number of nozzle injectors can be optionally changed without the need of conventional manufacturing methods. Angles can be adjusted for air nozzles with a high structural configuration type, instead of producing different nozzles. An air nozzle whose parts can be changed modularly and take



Figure 4: 3D model drawing of a modular jet-ring nozzle with 3 injectors

on a new shape will make the spinning process much easier. Such a system consists of a modular air nozzle, a modular top and bottom twisting chamber, a modular injector, a tangential adjustment bracket and a modular body (Figure 4).

2.3 Experimental setup

In the experimental study, conventional nozzles with the same structural configurations were produced to determine modular nozzle performance. Conventional nozzles were prepared for the same conditions as the modular nozzle, while the yarn production system was prepared simultaneously. The structural configurations of the developed modular nozzle were adjusted to result in a twist chamber diameter $\phi = 3$ mm and an injector diameter $\phi = 0.5$ mm, with three circumferential injectors. The only difference was the nozzle length. Since the modular jet-ring nozzle consisted of a mechanism, it had a length of 81 mm, i.e. three times the length of the conventional nozzle. According to the study by Guo et al., when other structural parameters of the nozzle are kept constant, the effects of injector position and nozzle length, respectively, on flow velocities, the axial velocities near the injection location and tangential velocities in all flow-regions do not change significantly due to the same initial swirl intensity [1]. Because the nozzle length did not affect the swirling flow, we concluded that the difference in the length of conventional and modular nozzles would not pose a problem. The structural configurations of the developed modular nozzle were adjusted to result in a twist chamber diameter $\phi = 3$ mm and an injector diameter $\phi = 0.5$ mm,



Figure 5: Jet-ring air nozzles mounted on conventional ring spinning machine

Table 1: Structural parameters of the conventional jet-ring nozzles and modular jet-ring nozzles

Nozzle type	Nozzle name	Twisting chamber diameter (mm)	Injector diameter (mm)	No. of injectors	Injector angle (°)
Conventional	C1	3	0.5	3	20
	C2	3	0.5	3	25
	C3	3	0.5	3	30
	C4	3	0.5	3	35
	C5	3	0.5	3	40
Modular	M1	3	0.5	3	20
	M2	3	0.5	3	25
	M3	3	0.5	3	30
	M4	3	0.5	3	35
	M5	3	0.5	3	40

with three circumferential injectors. The structural parameters of the jet-ring nozzles and modular jet-ring nozzle are shown in Table 1. Yarn production was performed on a Merlin SP43 conventional ring spinning machine made by the Pinter Group with a capacity of 16 spindles. The jet-ring air nozzles and modular jet-ring air nozzles mounted on the conventional ring spinning machine are illustrated in Figure 5.

2.4 Yarn production

One-hundred percent cotton yarns were produced in this experiment. We produced cotton jet-ring yarns of 19.6 tex (Table 2). In all the yarn productions, importance was given to working with the same spinning parameters, e.g., the same twist multiplier, draft,

Table 2: Fibre properties

Fibre properties	19.6 tex (Ne 30)
Staple length (mm)	30.53
Micronaire	4.52
U.I. (uniformity index)	85.7
Strength (cN/tex)	34.5
Breaking elongation (%)	6.4
SFI (short fibre index)	6.9
+b (yellowness)	7.9
Rd (reflectance degree)	72.1
CG (colour grade)	41–2
SCI (spinning count index)	160

spindle speed and traveller type (Table 3). In all jet-ring yarn productions, air pressure was set at two different values: 75 kPa (gauge) and 125 kPa (gauge). Z-twisted carded cotton yarns were produced on a conventional ring spinning machine with and without nozzle placement. The false-twist air vortex direction of the jet-ring nozzles also resulted in a Z-twist.

Table 3: Spinning particulars

Parameters	19.6 tex
Roving count (tex)	472
Twist (1/m)	830
α_e	3.7
Mean spindle speed (rpm)	13.000
Take up speed (m/min)	15.7
Traveller type	SFB 2.8 PM udr
Traveller ISO No.	31.5–50
Ring diameter (mm)	38
Draft/Break draft	1.181
Total draft	50.4

2.5 Yarn tests

Yarn hairiness, irregularity and imperfections tests were carried out using an Uster Tester 3. Tensile properties (percentage of elongation and tenacity measured as cN/tex) tests were carried out using an Uster Tensorapid. The cops and bobbins of each system were fed in the same order to the testers. Yarn test details are given in Table 4. The tests were carried out under the same atmospheric conditions

Table 4: Test particulars for each yarn sample

Yarn properties	Test device	Test length (m)	Test number	Total length (m)
Yarn irregularity and imperfections	Uster Tester 3	400	1	400
Yarn hairiness	Uster Tester 3	400	1	400
Tensile properties	Uster Tensorapid	0.5	10	5

(75 ± 5% RH and 25 ± 2 °C), and we conditioned samples for a minimum of seventy-two hours before the tests. All the tests were carried out on the same testers and test results were analysed statistically to determine any significant differences.

2.6 CFD study

In this part of the study, which is the numerical analysis section, an Ansys CFX 18.0 computational fluid dynamics program was used for both conventional nozzle and modular nozzle configurations. In his study, Yilmaz noted that the number of elements of around 400,000, depending on the nozzle geometry, produced sufficiently accurate results [17]. Approximately 2,500,000 tetrahedral elements are used for any geometry (conventional and modular nozzle type) in the mesh prepared for a parametric study (the number of elements varies according to structural parameters). Using an ICEM CFD mesher in the Ansys CFX 18.0, the body of influence and the thin mesh of size 0.07 mm element were assigned to the cylindrical control volume,. For the twisting chamber boundary layer, the size of the element was assigned a face sizing of 0.1 mm. A detail view of the conventional nozzle mesh topology is given in Figure 6, while modular nozzle mesh topology is given in Figure 7. After the parameters and mesh topology were determined, using the Ansys CFX 18.0 software, the inlet boundary condition was defined as 225 kPa (absolute) total pressure from the air inlet (injectors) (125 kPa gauge). The relative pressure value was defined as “0 kPa” by selecting static pressure in the outlet boundary condition. The opening boundary condition was defined in the fibre inlet opening and, similar to the outlet



Figure 6: Conventional nozzle mesh topology

boundary condition, the relative pressure value was defined as “0 kPa”. Air at 25° was selected as fluid and the reference pressure was defined as 100 kPa. All parametric study configurations were solved separately using an SST turbulence model.



Figure 7: Modular nozzle mesh topology

3 Results and discussion

3.1 Yarn hairiness results

The effect of conventional jet-ring nozzles and modular jet-ring nozzles on yarn hairiness (H) is shown in Figure 8. According to the yarn hairiness graph, the yarn hairiness value in conventional jet-ring nozzles was measured at the lowest 35° injector angle configuration at both pressure values. The second yarn hairiness value is followed by a 40° injector

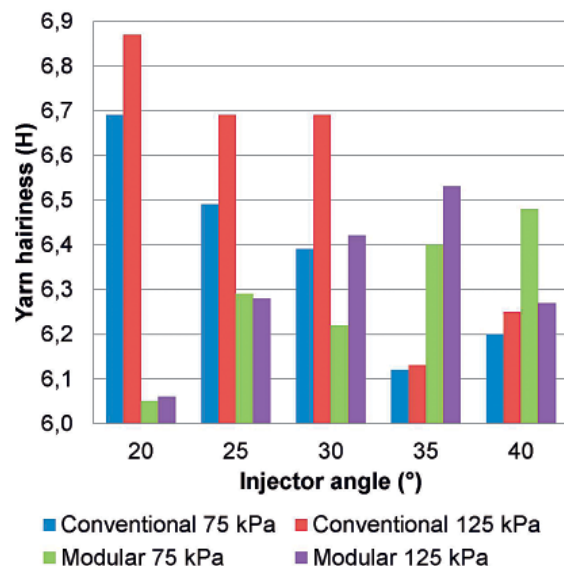


Figure 8: Comparison of conventional jet-ring nozzle and modular jet-ring nozzle yarn hairiness value

angle structural configuration. The worst yarn hairiness value in conventional jet-ring nozzles was obtained in the nozzle with a 20° injector angle configuration. Unlike conventional jet-ring nozzles, modular jet-ring nozzles achieved the best result when the yarn hairiness value was set to a 20° injector angle configuration. The worst yarn hairiness value achieved by modular jet-ring nozzles was obtained at a 35° injector angle configuration, which gives the best value for conventional jet-ring nozzles. When the hairiness value is considered, conventional jet-ring nozzles and modular jet-ring nozzles form an antithesis relative to one another in terms of the injector angle structural parameter. Comparing conventional jet-ring nozzles with modular jet-ring nozzles, it can be said that modular jet-ring nozzles are more successful in reducing hairiness. In modular and conventional nozzles with generally known structural configurations, an increase in pressure leads to an increase in yarn hairiness.

3.2 Yarn irregularity results

The effect of conventional jet-ring nozzles and modular jet-ring nozzles on yarn irregularity (% Cv m) is shown in Figure 9. An increase in pressure in conventional jet-ring nozzles with the tested structural configurations resulted in an increase in yarn irregularity. In modular jet-ring nozzles, an increase in pressure caused an increase in the yarn irregularity at the 20° and 35° injector angle values, while the other angle

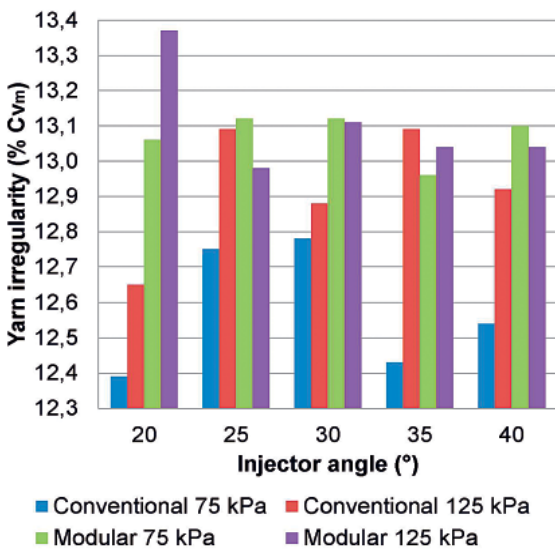


Figure 9: Comparison of conventional jet-ring nozzle and modular jet-ring nozzle yarn irregularity value

values showed an opposite decrease in yarn irregularity. In general, it is understood that the yarn irregularity values of the yarns produced in modular jet-ring nozzles are higher than those produced with conventional jet-ring nozzles.

3.3 Yarn elongation results

The effect of conventional jet-ring nozzles and modular jet-ring nozzles on yarn elongation (%) is shown in Figure 10. In conventional jet-ring nozzles with the tested structural configurations, there is a significant decrease in yarn elongation, except in the context of a pressure increase at the 40° injector angle. In modular jet-ring nozzles, an increase in pressure increased the yarn elongation value at the 20° and 25° injector angle values and decreased at other injector angle values. In general, it is understood that the yarn elongation values of the yarns produced using modular jet-ring nozzles are lower than those produced using conventional jet-ring nozzles.

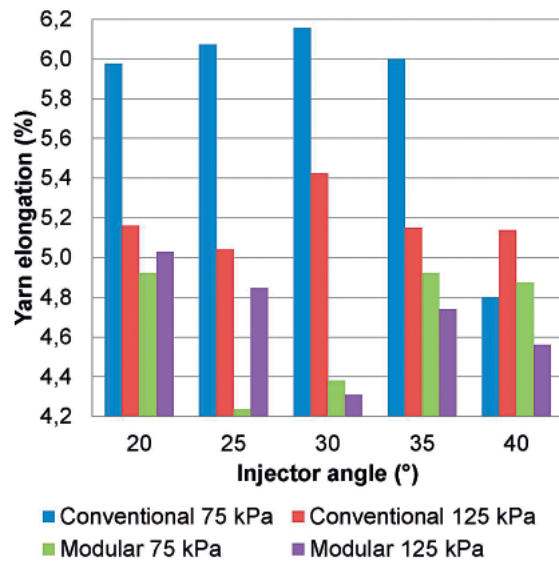


Figure 10: Comparison of conventional jet-ring nozzle and modular jet-ring nozzle yarn elongation value

3.4 Yarn tenacity results

The effect of conventional jet-ring nozzles and modular jet-ring nozzles on yarn tenacity (cN/tex) is shown in Figure 11. Increasing the pressure value in conventional jet-ring nozzles with the tested structural configurations showed a significant decrease in the yarn tenacity value as well as yarn elongation, except when the nozzle was set at a 40° injector angle. In

modular jet-ring nozzles, an increase in pressure increased yarn tenacity at 20°, 25° and 35° injector angle values and decreased at other injector angle values. When the air pressure was set to 75 kPa, the yarn tenacity values were higher in the yarns produced in conventional jet-ring nozzles, and higher in the yarns produced in modular jet-ring nozzles when it was set to 125 kPa. It was understood that modular jet-ring nozzles are less affected by a change in pressure in terms of the yarn tenacity value. This result showed that higher air pressure values can be achieved by using modular jet-ring nozzles without yarn breakage.

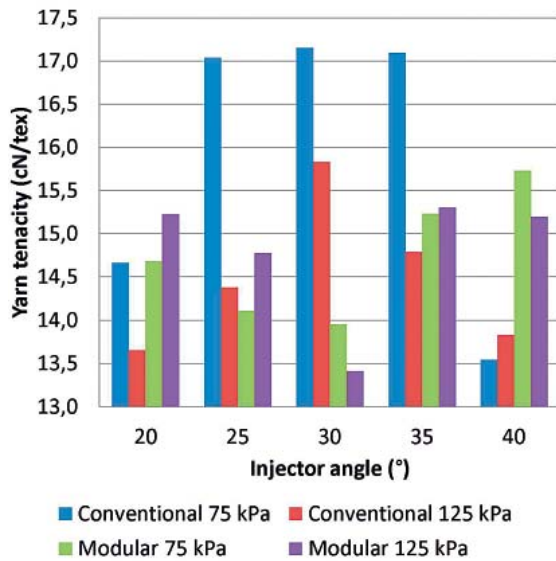


Figure 11: Comparison of conventional jet-ring nozzle and modular jet-ring nozzle yarn tenacity value

3.5 CFD result comparison

A CFD parameter comparison of conventional nozzles in five different injector angle configurations is given in Table 5, while a CFD parameter comparison of modular nozzles is given in Table 6. The swirl number, total pressure, flow pressure, Reynolds number, velocity, velocity in z axis, vorticity (curl of velocity) and helicity real eigen values of conventional and modular nozzles given in Table 5 and Table 6 are calculated in the plane where the injectors are opened to the twist chamber. The total pressure CFD result in the YZ plane of the five different conventional nozzle configurations given in Table 5 is shown in Figure 12. Similarly, the velocity CFD result is shown in Figure 13, the z-axis velocity CFD result is shown in Figure 14, the vorticity CFD result is shown in Figure 15, and the helicity real eigen CFD result is

shown in Figure 17. Also, vorticity flow trajectories are shown in Figure 16 and helicity real eigen flow trajectories are shown in Figure 18. Similarly, the total pressure CFD result in the YZ plane of the five different modular nozzle configurations given in Table 6 is shown in Figure 19, while the velocity CFD result is shown in Figure 20, the z-axis velocity CFD result is shown in Figure 21, the vorticity CFD result is shown in Figure 22, and the helicity real eigen CFD result is shown in Figure 24. Also, vorticity flow trajectories are shown in Figure 23 and helicity real eigen flow trajectories are shown in Figure 25.

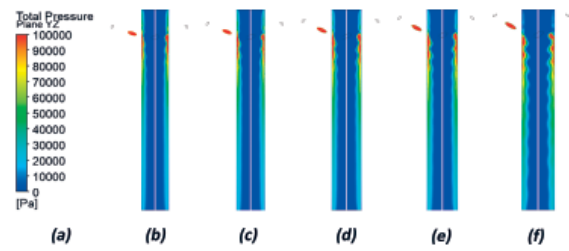


Figure 12: Conventional nozzle YZ plane total pressure CFD result: a) colour scale, b) injector angle 20°, c) injector angle 25°, d) injector angle 30°, e) injector angle 35°, f) injector angle 40°

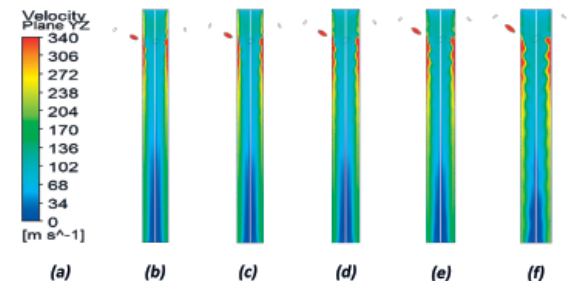


Figure 13: Conventional nozzle YZ plane velocity CFD result: a) colour scale, b) injector angle 20°, c) injector angle 25°, d) injector angle 30°, e) injector angle 35°, f) injector angle 40°

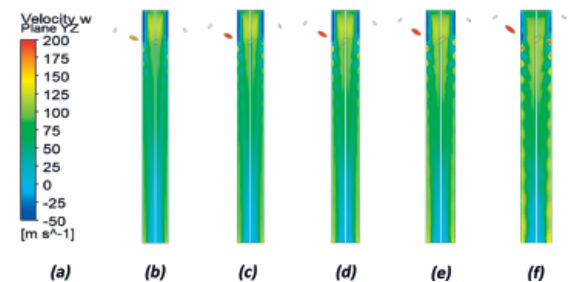


Figure 14: Conventional nozzle YZ plane velocity w (z axis) CFD result: a) colour scale, b) injector angle 20°, c) injector angle 25°, d) injector angle 30°, e) injector angle 35°, f) injector angle 40°

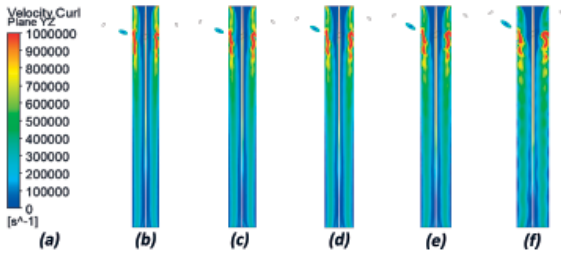


Figure 15: Conventional nozzle YZ plane vorticity (velocity curl) CFD result: a) colour scale, b) injector angle 20°, c) injector angle 25°, d) injector angle 30°, e) injector angle 35°, f) injector angle 40°

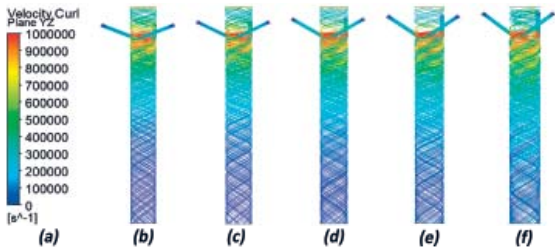


Figure 16: Conventional nozzle YZ plane vorticity (velocity curl) CFD result (flow trajectories): a) colour scale, b) injector angle 20°, c) injector angle 25°, d) injector angle 30°, e) injector angle 35°, f) injector angle 40°

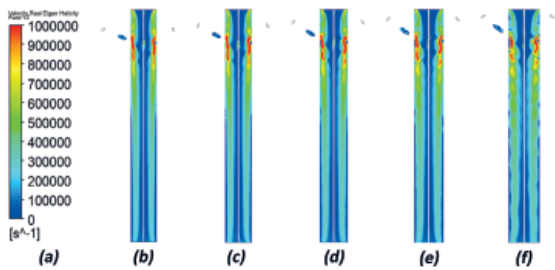


Figure 17: Conventional nozzle YZ plane helicity real eigen CFD result: a) colour scale, b) injector angle 20°, c) injector angle 25°, d) injector angle 30°, e) injector angle 35°, f) injector angle 40°

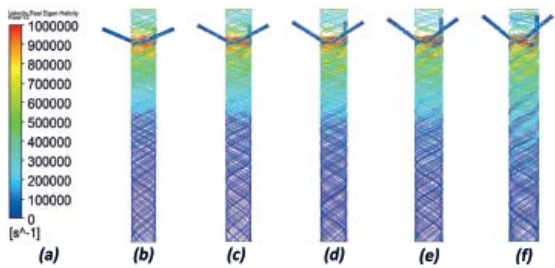


Figure 18: Conventional nozzle YZ plane helicity real eigen CFD result (flow trajectories): a) colour scale, b) injector angle 20°, c) injector angle 25°, d) injector angle 30°, e) injector angle 35°, f) injector angle 40°

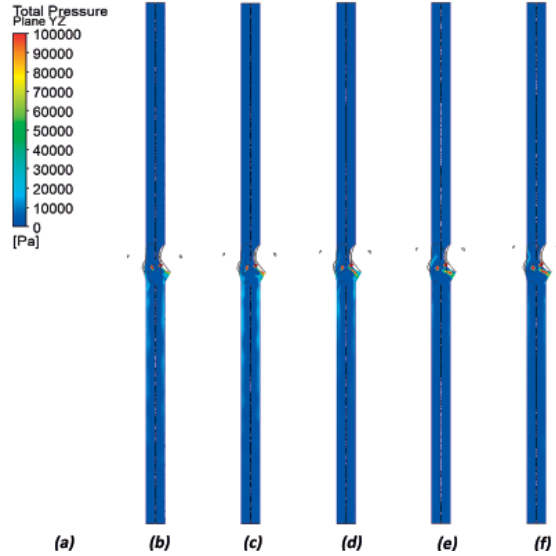


Figure 19: Modular nozzle YZ plane total pressure CFD result: a) colour scale, b) injector angle 20°, c) injector angle 25°, d) injector angle 30°, e) injector angle 35°, f) injector angle 40°

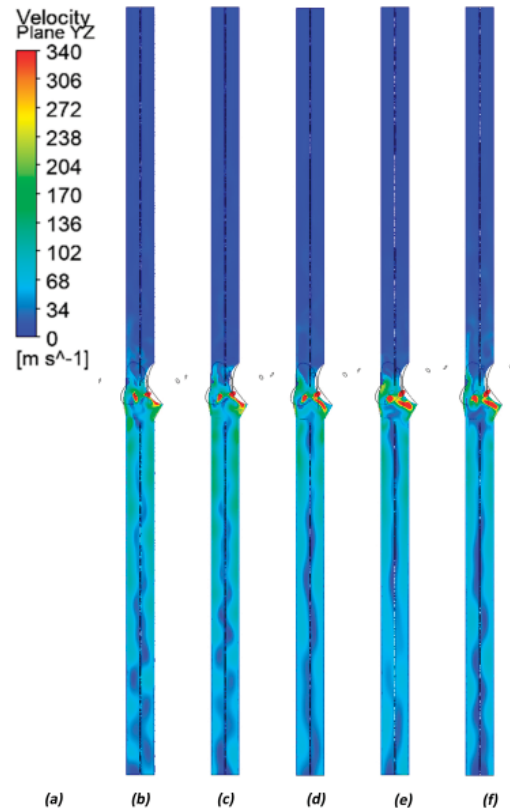


Figure 20: Modular nozzle YZ plane velocity CFD result: a) colour scale, b) injector angle 20°, c) injector angle 25°, d) injector angle 30°, e) injector angle 35°, f) injector angle 40°

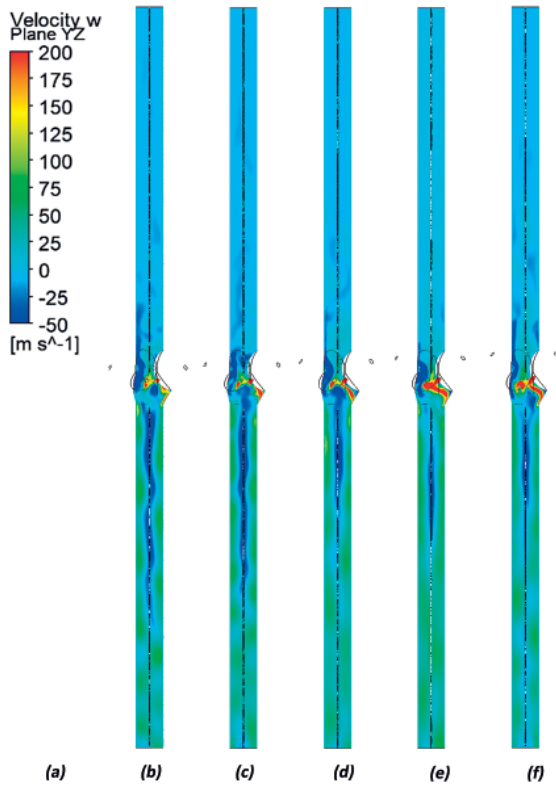


Figure 21: Modular nozzle YZ plane velocity w (z axis) CFD result: a) colour scale, b) injector angle 20° , c) injector angle 25° , d) injector angle 30° , e) injector angle 35° , f) injector angle 40°

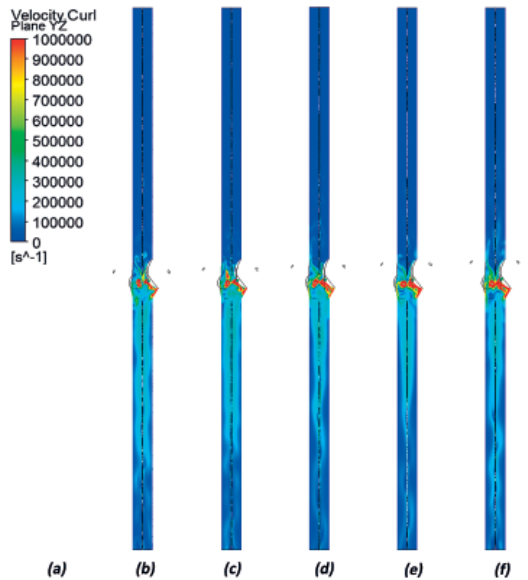


Figure 22: Modular nozzle YZ plane vorticity (velocity curl) CFD result: a) colour scale, b) injector angle 20° , c) injector angle 25° , d) injector angle 30° , e) injector angle 35° , f) injector angle 40°

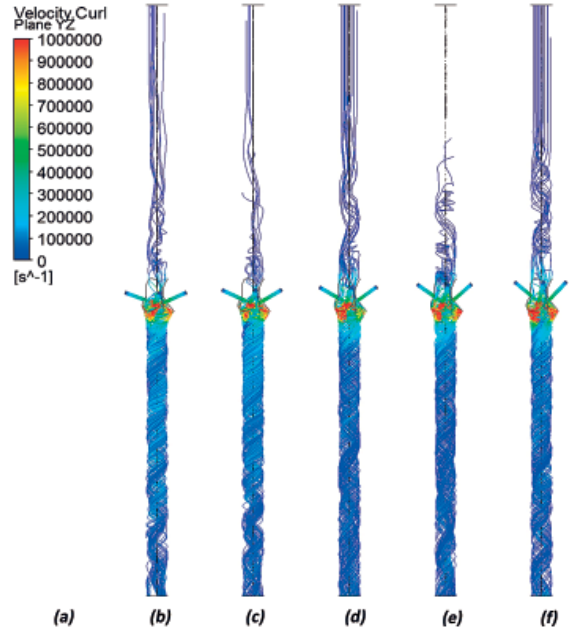


Figure 23: Modular nozzle YZ plane vorticity (velocity curl) CFD result: (flow trajectories) a) colour scale, b) injector angle 20° , c) injector angle 25° , d) injector angle 30° , e) injector angle 35° , f) injector angle 40°

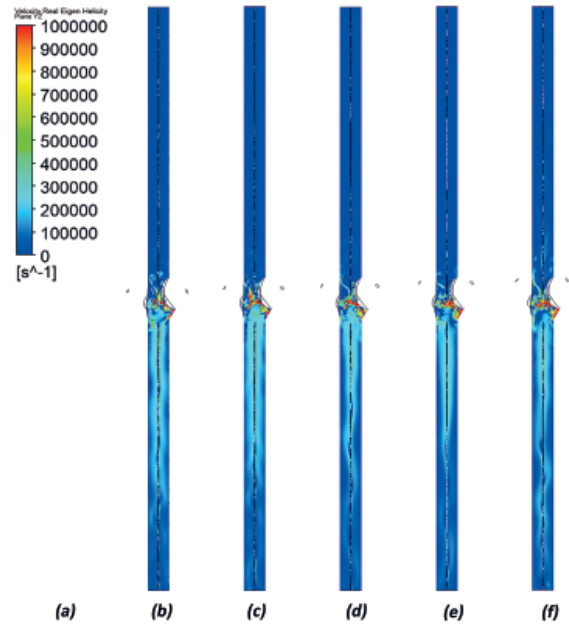


Figure 24: Modular nozzle YZ plane helicity real eigen CFD result: a) colour scale, b) injector angle 20° , c) injector angle 25° , d) injector angle 30° , e) injector angle 35° , f) injector angle 40°

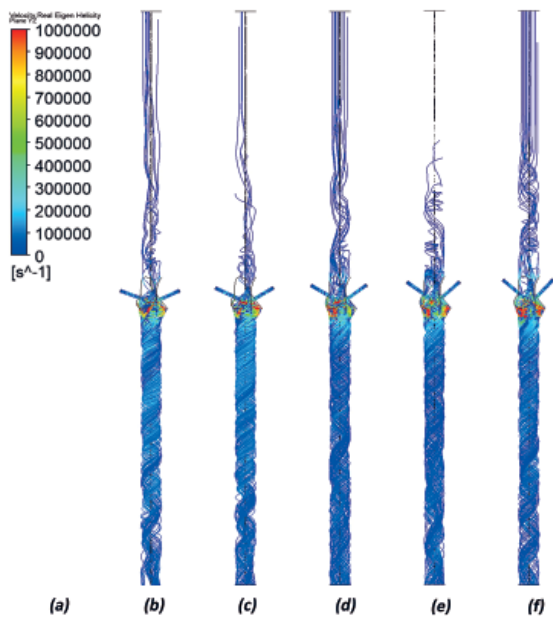


Figure 25: Modular nozzle YZ plane helicity real eigen CFD result (flow trajectories): a) colour scale, b) injector angle 20°, c) injector angle 25°, d) injector angle 30°, e) injector angle 35°, f) injector angle 40°

Considering injector air inlet mass flow values, the modular nozzles with the same structural configurations and analysed at the same pressure (225 kPa absolute) consumed an average of 11.5% more air than conventional nozzles. Considering fibre inlet mass flow values, an average suction in the fibre inlet opening of 0.77 times (minimum 0.65 – maximum 0.88)

the injector air inlet mass flow value was achieved from the fibre inlets of conventional nozzles. In modular nozzles, this coefficient was -0.05. In other words, in modular nozzles of the same structural configurations, air cannot be sucked in from the fibre inlet. Conversely, air is released the outside from this opening.

According to the principle of mass conservation, the mass flow rates of the fiber and the air outlet are the difference between the mass flow of air from the injectors and the mass absorbed from the fibers, if any, or the amount of air ejected from the fiber inlet.

In the conventional nozzle fiber inlet mass flow value is positive. In other words, air is discharged through this opening. In the modular nozzle, fiber inlet mass flow value is a negative. In this case, we understand that there is air suction from the environment to the twisting chamber.

The air flow velocity value of the modular nozzle configurations and the velocity-dependent z-axis velocity, Reynolds number, vorticity and helical real eigen values were approximately one third of that of conventional nozzles. Although the swirl numbers (S_n) of the modular nozzle configurations given in Table 6 are lower than the conventional nozzles, the geometric swirl numbers (S_g) are relatively high compared to the conventional nozzles (Table 5).

According to the calculations made in the plane in which the injectors are opened to the twisting chamber in the comparative structural configurations, the total pressure values of conventional nozzles are

Table 5: CFD analysis results of conventional nozzles with twisting chamber diameter $\phi = 3$ mm, injector diameter $\phi = 0.5$ mm and three circumferential injectors (225 kPa absolute)

Injector angle (degree)	20	25	30	35	40
Injector air inlet mass flow rate (kg/s)	0.000336	0.000343	0.000349	0.000358	0.000376
Fibre inlet mass flow rate (kg/s)	0.000217	0.000241	0.000267	0.000301	0.000332
Fibre and air outlet mass flow rate (kg/s)	-0.000553	-0.000584	-0.000616	-0.000659	-0.000708
Swirl number (S_n)	3.38	3.175	2.908	2.626	2.308
Geometric swirl number (S_g)	4.166	3.746	3.333	2.903	2.597
Total pressure (Pa)	44161	42443	41943	41793	41972
Flow pressure (Pa)	6375	7625	8576	9075	9399
Reynolds number (Re)	39820	39047	39543	40456	41238
Velocity (m/s)	202.9	201.1	203.7	208.4	212.4
Velocity w (fibre axis) (m/s)	64.7	68.6	72.5	77.6	84.4
Vorticity	708257	687890	675408	675006	682107
Helicity real eigen	599981	574558	541261	537100	522006

Table 6: CFD analysis results of modular nozzles with twisting chamber diameter $\phi = 3$ mm, injector diameter $\phi = 0.5$ mm and three circumferential injectors (225 kPa absolute)

Injector angle ($^{\circ}$)	20	25	30	35	40
Injector air inlet mass flow rate (kg/s)	0.000375	0.000394	0.000397	0.000397	0.000399
Fibre inlet mass flow rate (kg/s)	-0.000049	-0.000018	-0.000011	-0.000024	0.000010
Fibre and air outlet mass flow rate (kg/s)	-0.000326	-0.000375	-0.000386	-0.000374	-0.000410
Swirl number (S_n)	0.433	0.395	0.306	0.343	0.348
Geometric swirl number (S_g)	14.92	11.968	10.972	11.114	8.71
Total pressure (Pa)	-493	1026	-428	-650	143
Flow pressure (Pa)	-1036	72	-1934	-2539	-1390
Reynolds number (Re)	12552	14671	9359	11246	9666
Velocity (m/s)	64.6	75.6	48.2	57.9	49.8
Velocity w (fibre axis) (m/s)	14.2	10.1	21	16.6	24.2
Vorticity	225448	223036	197273	233608	230605
Helicity real eigen	172484	156333	138241	171569	171734

above 40 kPa, while the total pressure value in modular nozzles is just below or just above 0 kPa. Similarly, the flow pressure value of conventional nozzles is above 6 kPa, while the flow pressure value of modular nozzles is below 0 kPa.

According to the graphical comparison of yarn hairiness of the modular nozzles and conventional nozzles in Figure 8, modular nozzles with a pressure of 125 kPa (225 kPa absolute) demonstrated the lowest yarn hairiness at injector angle configurations of 20°, 40°, 25°, 30° and 35°. According to the modular nozzle YZ plane vorticity CFD result in Figure 22, the order of vorticity from highest value to lowest value is seen at injector angle configurations of 20°, 25°, 30°, 35° and 40°. If the measurement at 40° in Figure 8 is not taken into account, the increase in the amount of vorticity resulted in a decrease in yarn hairiness. A similar situation was seen in the helicity real eigen CFD results in the YZ plane (Figure 24).

According to the graphical comparison of yarn hairiness of the modular nozzles and conventional nozzles in Figure 8, conventional nozzles with a pressure of 125 kPa (gauge) demonstrated the lowest yarn hairiness at injector angle configurations of 20°, 40°, 25°, 30° and 35°. According to the modular nozzle YZ plane vorticity CFD result in Figure 15, the order of vorticity from highest value to lowest value is seen at injector angle configurations 40°, 35°, 30°, 25° and 20°. A similar situation was seen in the helicity real eigen CFD results in the YZ plane (Figure 17).

3.6 CFD verification

The CFD validation process was addressed and validated in a study similar to this one [11].

4 Conclusion and outlook

- Comparing conventional jet-ring nozzles with modular jet-ring nozzles in terms of yarn hairiness value, modular jet-ring nozzles proved to be more successful in reducing yarn hairiness values. The main objective of jet-ring nozzles is to reduce yarn hairiness values.
- When hairiness values are considered, conventional jet-ring nozzles and modular jet-ring nozzles form an antithesis relative to one another in terms of the injector angle structural parameter. In the 20° injector angle structural configuration, conventional jet-ring nozzles gave the best yarn hairiness values, while modular jet-ring nozzles gave the worst yarn hairiness values. In the 35° injector angle structural configuration, hairiness values were reversed. In other words, modular and conventional nozzles formed an antithesis with respect to one another in terms of yarn hairiness values according to their injector angle structural configurations.
- In modular and conventional nozzles with generally known structural configurations, an increase in pressure led to an increase in yarn hairiness.
- It is generally understood that the irregularity values of yarns produced using modular jet-ring

nozzles are higher than those produced using conventional jet-ring nozzles.

- It is generally understood that the elongation values of the yarns produced using modular jet-ring nozzles are lower than those produced using conventional jet-ring nozzles.
- When the air pressure was set to 75 kPa (gauge), yarn tenacity values were higher in the yarns produced using conventional jet-ring nozzles, and higher in the yarns produced in modular jet-ring nozzle when it was set to 125 kPa (gauge).
- Comparing the flow parameters of yarn hairiness (CFD analysis), it was found that increasing vorticity or helicity real eigen values reduced yarn hairiness. Yarn hairiness can be minimised if both conventional nozzles and modular nozzles concentrate on structural configurations that can maximise vorticity or helicity real eigen values to reduce yarn hairiness.
- According to the structural configurations that maximise vorticity or helicity real eigen values in conventional nozzles, the twisting chamber diameter should be at the lowest value ($\phi = 2$ mm).
- No significant correlation was found between other structural parameters and vorticity or helical real eigen values in conventional nozzles. However, in conventional nozzles, vorticity or helical real eigen values were high in the 35–40° injector angle configurations.
- In modular nozzles, on the contrary, vorticity or helical real eigen values were high in the 20–25° injector angle configurations and low in the 35–40° injector angle configurations.
- It is precisely for this reason that the yarn produced using modular nozzles demonstrated a low hairiness value when a low injector angle was set and a high hairiness value when a high injector angle was set, which can be explained logically when comparing vorticity or helicity real eigen values.

Acknowledgement

This work was supported by grants from the Unit of Scientific Research Projects of Isparta (Suleyman Demirel University) in Turkey [Project 4995-D1-17]. We would like to thank H. Husnu Isik, the owner of Adim Textile Industry and Trade Inc. (Isparta, Turkey), and Ayse Korkut, the production manager at Adim Textile Industry and Trade Inc., for support in yarn production and yarn hairiness testing. The authors also wish to express their thanks to Umit Tasdeler for his collaboration.

References

1. GUO, Hui-Fen, YU, Chong-Wen, XU, Bin-Gang, LI, Sheng-Yan. Effect of the geometric parameters on a flexible fibre motion in a tangentially injected divergent swirling tube flow. *International Journal of Engineering Science*, 2011, **49**(10), 1033–1046, doi: 10.1016/j.ijengsci.2011.06.002.
2. YILMAZ, Demet, USAL, Mustafa Resit. A comparison of compact-jet, compact, and conventional ring-spun yarns. *Textile Research Journal*, 2011, **81**(5), 459–470, doi: 10.1177/00405175110385174.
3. WANG, Xungai, MIAO, Menghe, HOW, Yanlai. Studies of JetRing spinning. Part I: reducing yarn hairiness with the JetRing. *Textile Research Journal*, 1997, **67**(4), 253–258, doi: 10.1177/004051759706700403.
4. *Ansys fluent theory guide*. Canonsburg : Ansys, 2001, p. 868.
5. AKANSU, Selahaddin Orhan. Heat transfers and pressure drops for porous-ring turbulators in a circular pipe. *Applied Energy*, 2006, **83**(3), 280–298, doi: 10.1016/j.apenergy.2005.02.003.
6. EBERLINC, Matjaž, ŠIROK, Brane, HOČEVAR, Marko, DULAR, Matevž. Numerical and experimental investigation of axial fan with trailing edge self-induced blowing. *Forsch im Ingenieurwesen / Engineering Research*, 2009, **73**(3), 129–138, doi: 10.1007/s10010-008-0086-8.
7. MANI, Sivabalan, SANAL, Kumar V.R. 3D flow visualization and geometry optimization of cavity based scramjet combustors using k- ω model. In *51st AIAA/SAE/ASEE Joint Propulsion Conference*. (AIAA Propulsion and Energy Forum). Reston : American Institute of Aeronautics and Astronautics, 2015, doi: 10.2514/6.2015-3946.
8. SHAHĪD, Mahmood, HUANG, De-Bo. Resistance calculations of trimaran hull form using computational fluid dynamics. In *Proceedings : Fourth International Joint Conference on Computational Sciences and Optimization, CSO 2011*. Los Alamitos : CPS, 2011, 81–85, doi: 10.1109/CSO.2011.225.
9. ŠIMIC, Marko, HERAKOVIČ, Niko. Reduction of the flow forces in a small hydraulic seat valve as alternative approach to improve the valve characteristics. *Energy Conversion and Management*, 2015, **89**, 708–718, doi: 10.1016/j.enconman.2014.10.037.

10. DENG, Ruoyu, JIN, Yingzi, KIM, Heuy Dong. Numerical simulation of the unstart process of dual-mode scramjet. *International Journal of Heat and Mass Transfer*, 2017, **105**, 394–400, doi: 10.1016/j.ijheatmasstransfer.2016.10.004.
11. GULSEVINCLER, Ekrem, USAL, Mustafa Resit, YILMAZ, Demet. The effects of structural parameters on tangentially injected highly swirling turbulent tube air flow. *SN Applied Sciences*, 2019, **1**(8), 1–26, doi: 10.1007/s42452-019-0850-4.
12. YILMAZ, Demet, USAL, Mustafa Resit. Effect of nozzle structural parameters on hairiness of compact-jet yarns. *Journal of Engineered Fibers and Fabrics*, 2012, **7**(2), 56–65, doi: 10.1177/155892501200700209.
13. YILMAZ, Demet, USAL, Mustafa Resit. A study on siro-jet spinning system. *Fibres and Polymers*, 2012, **13**(10), 1359–1367, doi: 10.1007/s12221-012-1359-2.
14. YILMAZ, Demet, USAL, Mustafa Resit. Improvement in yarn hairiness by the siro-jet spinning method. *Textile Research Journal*, 2013, **83**(10), 1081–1100, doi: 10.1177/0040517512471748.
15. SU, Xuzhong, LIU, Xinjin, LIU, Xiaoyan. Numerical simulation of flow field in the pneumatic compact spinning systems using finite element method. *International Journal of Clothing Science and Technology*, 2018, **30**(3), 363–379, doi: 10.1108/IJCST-11-2017-0180.
16. GULSEVINCLER, Ekrem, USAL, Mustafa Resit, YILMAZ, Demet. Effects of nozzle structural parameters on yarn hairiness in jet-ring spinning system. *The Journal of the Textile Institute*, 2020 (in press), 1–11, doi: 10.1080/00405000.2020.1716527.
17. YILMAZ, Demet. Development and numerical modelling of plied yarn production process based on the usage of high velocity air. *Ph.D. thesis*. Isparta : Suleyman Demirel University, 2011.